Impact of Ionic Liquids in Aqueous Solution on Bacterial Plasma Membranes Studied with Molecular Dynamics Simulations

Geraldine S. Lim[a], Jernej Zidar[a], Daniel W. Cheong[a], Stephan Jaenicke[b], Marco Klähn[c]*

[a] Institute of High Performance Computing, Agency for Science, Technology and Research, 1 Fusionopolis Way, #16-16, Connexis, Singapore 138632, Rep. of Singapore

[b] National University of Singapore, Department of Chemistry, 3 Science Drive 3, Singapore 117543, Rep. of Singapore

[c] Institute of Chemical and Engineering Sciences, Agency for Science, Technology and Research, 1 Pesek Road, Jurong Island, Singapore 627833, Rep. of Singapore

E-mail: klahnm@ices.a-star.edu.sg

Abstract

The impact of five different imidazolium-based ionic liquids (ILs) diluted in water on the properties of a bacterial plasma membrane is investigated using molecular dynamics (MD) simulations. Cations considered are 1-octyl-3-methylimidazolium (OMIM), 1-octyloxymethyl-3-methylimidazolium (OXMIM) and 1-tetradecyl-3-methylimidazolium (TDMIM) as well as the anions chloride and lactate. The atomistic model of the membrane bilayer is designed to reproduce the lipid composition of the plasma membrane of gram-negative *Escherichia coli*. Spontaneous insertion of cations into the membrane is observed in all ILs. Substantially more insertions of OMIM than of OXMIM occur and the presence of chloride reduces cation insertions compared to lactate. In contrast, anions do not adsorb onto the membrane surface

nor diffuse into the bilayer. Once inserted, cations are oriented in parallel to membrane lipids with cation alkyl tails embedded into the hydrophobic membrane core, while the imidazolium-ring remains mostly exposed to the solvent. Such inserted cations are strongly associated with one to two phospholipids in the membrane. The overall order of lipids decreased after OMIM and OXMIM insertions, while on the contrary the order of lipids in the vicinity of TDMIM increased. The short alkyl tails of OMIM and OXMIM generate voids in the bilayer that are filled by curling lipids. This cation induced lipid disorder also reduces the average membrane thickness. This effect is not observed after TDMIM insertions due to the similar length of cation alkyl chain and the fatty acids of the lipids. This lipid-mimicking behavior of inserted TDMIM indicates a high membrane affinity of this cation that could lead to an enhanced accumulation of cations in the membrane over time. Overall, the simulations reveal how cations are inserted into the bacterial membrane and how such insertions change its properties. Moreover, the different roles of cations and anions are highlighted and the fundamental importance of cation alkyl chain length and its functionalization is demonstrated.

Keywords

Ionic liquid, membrane, antimicrobial, molecular dynamics simulations, lipid bilayer, imidazolium

1. Introduction

The occurrence of multi-drug resistant bacteria in recent years has motivated the search for novel antimicrobial compounds. Multi-drug resistant bacteria remain active even after antibiotic treatment, which is a cause of major concern. In fact, the World Health Organization (WHO) identified combating antimicrobial resistance as their theme in 2011.[1]

One promising line of research is the study of antimicrobial peptides (AMPs). AMPs are essential antibiotic host defense peptides commonly found in nature.[2] Their widespread presence in multicellular organisms demonstrate their importance throughout evolution.[3]

AMPs are typically short peptides, comprised of less than 50 amino acid residues.[2,4,5] AMPs are amphipathic molecules that contain polar and hydrophobic amino acids with an overall positive charge. Although many types of AMPs with substantially different structures have been found, some common features can be identified such as the cationic charge and amphiphilic properties. The amphiphilicity of AMPs enables insertion into cell membranes, since the positively charged region interacts favorably with the negatively charged surface of the bacterial cell, while the hydrophobic residues facilitate interactions with lipids inside the cell membrane.

The main difference between mammalian and bacterial cells is the presence of anionic phospholipids on the outer leaflet of the lipid bilayer in bacterial cells.[3,6] Mammalian cells, on the other hand, carry predominantly zwitterionic phospholipids in the outer leaflet, resulting in an overall neutral charge of the lipid bilayer. AMPs take advantage of this fundamental difference in membrane composition to selectively affect only bacterial cells. Since AMPs target the lipids in the bacterial membrane rather than specific targets within the cell, developing bacterial resistance is more difficult.[3,7,8] However, despite AMPs being promising agents, only a handful are currently in clinical use.[5,6,9] Some reasons include susceptibility to protease degradation and their inability to cross certain membranes such as the blood brain barrier (BBB), to name only a few drawbacks.[6,8,10,11]

Nevertheless, it has been widely recognized that the use of AMPs or related compounds have good prospects for combating antimicrobial resistance. A potentially viable alternative to AMPs are suitable ionic liquids (ILs), which share some properties that are essential for antimicrobial capabilities of AMPs. ILs are salts solely composed of ions with low melting points that often remain liquid even below room temperature. Delocalization of charge over large parts of the ions weakens attraction between counter ions, and together with structural ion asymmetry, a low melting point below room temperature can be obtained. ILs possess many favorable properties such as negligible vapor pressure, non-flammability, chemical and thermal stability.[12-14] Some of the commonly used ions include cations based on imidazolium, pyridinium or ammonium, as well as halides, tetrafluroborate and bis(trifluoromethanesulfonyl) amide for anions. Members of the newest generation of ILs are frequently composed of organic

compounds only, such as ionic amino acids or lactate for instance. In any event, ILs are highly tunable solvents, since independent modifications of cations and anions can be made, giving rise to task specific solvents.[12,15] It has been demonstrated that slight modifications to the constituent ions are sufficient to effect a substantial change in chemical and physical properties.[16-18]

The vast amount of possible ionic constituents and the possibility to modify cations and anions independently have enabled the design of fully biocompatible, biodegradable, non-toxic and recyclable ILs[19-28] that could hence also be suitable as components in drugs. For instance, it was found that incorporating ester or amide functional groups in the design of cations can improve its biodegradability.[25,27,29] Moreover, biocompatibility has also been demonstrated by the ability of suitable ILs to preserve the structure and functionality of proteins or even entire cells that were wholly immersed in ILs, which led to various applications in biocatalysis.[30,31]

Indeed, it has been found that some ILs exhibit pronounced antimicrobial properties.[24,32-35] This was not unexpected, because their structurally similar counterparts, quaternary ammonium compounds (QACs), have been well studied in the field of surfactants with antiseptic properties.[36] In fact, the minimal inhibitory concentration (MIC) values for imidazolium, pyridinium, phosphonium and ammonium-based ILs regarding various types of bacteria and fungi show improved antimicrobial activities relative to conventional antimicrobial agents.[24,28,36,37] This antimicrobial activity has been found to be closely related to the length of the alkyl chain of the cation, with longer chains exhibiting greater antimicrobial efficacy.[12,34,37] However, this biological efficacy does not increase indefinitely with increasing chain length, and this phenomenon has been referred to as the cutoff effect.[26,37] Possible explanations proposed for this reduced efficacy include insufficient solubility and micellization of the cations and assimilation of the long chained cations into the membrane.[37] The optimum chain length has been found to be typically between 12 to 16 carbons, depending on the cation head group.[32,38] Functionalization also alters the antimicrobial activity of ILs. For instance, the inclusion of polar groups to the cation alkyl chain serves to lower toxicity and antimicrobial efficacy.[26,27] Anions, on the other hand, seem to play only a secondary role in determining antimicrobial

activity.[26,32,37] Overall, so far reported results in combination with the realization that only a very small fraction of possible ILs have even been synthesized so far, demonstrate that the design of effective antimicrobial ILs that do not harm mammalian cells nor pose serious environmental risks is achievable.

Although many experiments have demonstrated the antimicrobial efficacy of ILs, an understanding of the mechanism behind the observed antimicrobial activity of ILs remains unclear. Such an understanding, however, is essential to guide the design of improved ILs that increase antimicrobial effectiveness as well as selectivity further, considering the virtually infinite number of ILs that could be generated. Therefore, detailed computational models that simulate ILs in contact with bacterial surfaces, i.e. their plasma membranes, provide an important complementing method. The main aim eventually is to find relationships that connect basic ion properties with antimicrobial activity and selectivity. Some studies that applied molecular dynamics (MD) simulations to analyze the impact of ILs on model membranes have already been reported: Cromie *et al.* studied the interactions of 1-butyl-3-methylimidazolium ILs with a cholesterol bilayer and observed cation adsorption at the water – cholesterol interface.[39] Bingham and Ballone investigated the effect of 1-butyl-3-methylimidazolium based ILs on a membrane composed of POPC phospholipids, and observed cations that diffused with their alkyl tail first into the bilayer.[40] Klähn and Zacharias studied the insertion of 1-octyl-3-methylimidazolium cations into membrane models of cancerous and healthy cells, whereby they identified a protective function of additional cholesterol in membranes of healthy cells that impeded cation insertion.[41]

In the present work, we studied the interactions of ILs in aqueous solution with a phospholipid bilayer model based on *E. coli*. We used an all-atomistic model in combination with MD simulations and an empirical molecular mechanical (MM) force field. The structure, dynamics and energetics of the membrane – IL systems were analyzed to study varying effects that the ILs induced on the membrane. Considered cations were based on imidazolium, the so far most commonly used type of cations in ILs with demonstrated antimicrobial activities. To study the observed alkyl chain length effect we included cations with octyl (n=8) and tetradecyl (n=14)

chains. Shorter alkyl chains do not display much antimicrobial activity and were thus not considered in this study.[36-38,42] Also a cation that involved an ether group in its alkyl chain was included in this study to investigate alkyl chain functionalization, which has been reported to effect antimicrobial activity.[24,26] These cations were paired with chloride and lactate to study the effect of anion variation on the membrane, even though these effects are expected to be notably less pronounced.[32,43]

The results of this study will provide indications for the underlying reasons behind observed variations of antimicrobial activity. The results will additionally also be relevant for the study of potential general toxicity of ILs, which is a property that is closely related to antimicrobial activity.

2. Methodology

2.1 Ionic Liquid Force Field

Molecular mechanical (MM) all-atomistic force fields were used to calculate the potential energy and the functional form in eq. 1 was used:

$$E_{pot} = \sum_{i,j}^{bonds} k_{ij}\ (l_{ij} - l_{0,ij})^2 + \sum_{i,j,k}^{angles} k_{ijk}\ (\varphi_{ijk} - \varphi_{0,ijk})^2$$

$$+ \sum_{i,j,k,l}^{improper} k_{ijkl}\ (\theta_{ijkl} - \theta_{0,ijkl})^2 + \sum_{i,j,k,l}^{torsions} E_{ijkl}\ \left[1 + \cos\ (n_{ijkl}\,\phi_{ijkl} - \delta_{0,ijkl})\right] \qquad (1)$$

$$+ \sum_{i,j} \frac{q_i q_j e^2}{4\pi\varepsilon_0 r_{ij}} + 4\varepsilon_{ij}\left[\left(\frac{\sigma_{ij}}{r_{ij}}\right)^{12} - \left(\frac{\sigma_{ij}}{r_{ij}}\right)^{6}\right]$$

The first four terms constitute bonded interactions which describe vibrations along bonds, angles and rotation around bonds, while the last two terms describe the non-bonded interactions. The fifth and sixth term respectively refers to the electrostatic Coulomb potential

and Lennard Jones potential. The latter includes contributions from both the attractive (van der Waals interactions) and repulsive (Pauli exclusion interactions) terms.

The ILs were described using the CHARMM General Force Field (CGenFF).[44] Ions included in this study are: 1-octyl-3-methylimidazolium (OMIM), 1-tetradecyl-3-methylimidazolium (TDMIM), 1-octyloxymethyl-3-methylimidazolium (OXMIM), chloride (Cl) and lactate (Lact). All combinations were simulated, with the exception of TDMIM-Cl, giving rise to a total of 5 ILs. Henceforth, only the abbreviations of the ILs will be used. Figure 1 illustrates all ions comprising the selected ILs.

Initial assignment of atom types and corresponding parameters for atom, bond, angle and dihedral potentials was carried out using the portal Paramchem.[45,46] This portal requires as input a list of atoms and their coordinates for considered ions. The portal uses this information to perform a similarity search by comparing these new compounds with already parameterized compounds from a database. Found similarity is indicated by a penalty score determined by Paramchem that is associated with every parameter. In the case of the ILs surveyed in this study, satisfactory similarity was found for all parameters, except for partial atomic charges, which were hence recalculated using quantum chemical calculations with second order Møller–Plesset perturbation (MP2) and the 6-31+G(d) Pople basis set. Partial charges were derived by fitting the electrostatic potential induced by the continuous charge distribution with the Merz-Singh-Kollman scheme (ESP charges).[47,48] All atom types and charges used are shown in Table S1 in Supporting Information. The Gaussian 09 software package was used for this calculation.[49]

This study involves the migration of some ions from the solvent (water) to the membrane. The highly charged region of the cations, i.e. imidazolium ring, remains partially solvated even after insertion into the membrane, while the alkyl tail, which is less sensitive to changes in the environment, lies among the phospholipids. The anions remain solvated in water throughout the simulation. Thus, it is appropriate to calculate the partial charges of these ions in water. The polarizable continuum model (PCM) was utilized, and a dielectric constant for water was specified.[50] The partial charges for all ions included in this study are shown in Figures S1-S4 in the Supporting information.

IL parameterization was first benchmarked through a comparison between computed and experimental mass densities. Simulations containing *pure* ILs were performed for 50 ns, and their densities were computed. IL densities were averaged over the last 10 ns. We compared densities in the two cases where experimental densities were available, namely for OMIM-Cl and EMIM-Lact. It was found that computed densities deviated less than 4% from measured values, demonstrating that bonded interaction parameters were adequately chosen.[51,52] Therefore, based on the agreement obtained with existing results and high similarity scores for all bonded interaction parameters according to Paramchem, we conclude that the applied force field is adequate for the description of considered ions.

2.2 *E. coli* Model Membrane

In this study, a model for the *E. coli* plasma membrane was constructed, for which the lipid composition was obtained from literature according to references:[53,54] 80 mol % phosphatidylethanolamine (PE), 15 mol % phosphatidylglycerol (PG) and 5 mol % phosphatidic acid (PA). Therefore, three different types of phospholipids were incorporated in a phospholipid bilayer model: 1-palmitoyl-2-oleoyl-*sn*-glycero-3-phosphoethanolamine (POPE), 1-palmitoyl-2-oleoyl-*sn*-glycero-3-phosphoglycerol (POPG) and 1-palmitoyl-2-oleoyl-*sn*-glycero-3-phosphatidic acid (POPA). Figure 2 shows the *E. coli* membrane model used in this study. Henceforth, the terms membrane and bilayer will be used interchangeably, and the *E. coli* membrane model is designated as M_{EC} in this work.

In this work, we investigated direct interactions of ILs with the membrane surface. Specific IL interactions with embedded transmembrane proteins or lipopolysaccharides (LPS) were not considered. Due to the small size of considered ions and strong interactions between cations and the negatively charged membrane surface, direct contact between a fraction of solvated ILs and phospholipids of the membrane bilayer appear to be inevitable, despite the otherwise observed protective function of the LPS layer.[28,55] Any found changes in membrane properties induced by such direct interactions would be indicative of an antimicrobial effect, without

excluding possible additional antimicrobial effects induced by interactions with other membrane components.

The model membrane was constructed using the portal CHARMM-GUI.[56-59] The portal generates a membrane structure based on the specified molar ratios of phospholipids in the bilayer and the chosen size of the membrane. The algorithm takes into account the size of the desired lipid molecules, which greatly simplifies the process of generating an initial membrane structure. The lipid components of the *E. coli* membrane were parameterized and validated previously, thus no additional validation was necessary.[60-64] The lipid molecule parameterization is part of the CHARMM36 force field.[65] The model membrane was then solvated using TIP3P water molecules.[66] Electroneutrality of the negatively charged membrane was achieved by adding sodium ions accordingly.

2.3 Simulated Membrane – IL Systems

Each M_{EC} – IL system contained approximately 24,000 atoms, with 9,988 atoms belonging to the bilayer. The individual composition of each system can be found in Table 1. A total of 80 phospholipids in the bilayer, namely POPE, POPG and POPA were included, with the composition stated in the previous section. An IL concentration of 0.25 M was fixed across all systems, equivalent to twenty ion pairs randomly placed in the solvent. The negative charges on the surface of the bacterial membrane would lead to a local concentration of cations that is larger than in the aqueous solution. Also, using a larger ion concentration in our model makes the impact of IL on membranes more clear.

Only for the TDMIM-Lact system, a lower IL concentration was used, arising from its propensity to form cation aggregates. In this system, when twenty ion pairs were incorporated, cation aggregates formed due to hydrophobic interactions since TDMIM contain long non-polar alkyl chains, resulting in only few freely solvated cations available for membrane insertion. Hence, ion pairs were added only gradually during the course of the simulation, so as to avoid a situation where a high cation concentration in the solvent prevents cation insertion into

membranes due to aggregation. The ion concentration was gradually increased during the course of a 50 ns MD simulation from 0.02 M to 0.07 M for this system.

2.4 Specifications of MD simulations

Classical all-atomistic MD simulations were performed in this study with the software package GROMACS.[67,68] The leap-frog algorithm was used to integrate the equations of motion, with a time step of 2 fs. Bond lengths involving hydrogen atoms were restrained with the LINCS algorithm.[69] Periodic boundary conditions were applied to the cuboid boxes. The Nosé-Hoover thermostat was used, with a reference temperature of 300 K and a time constant of 0.5 ps.[70,71] Semi-isotropic coupling was applied for pressure control, whereby the x and y coordinates (in the plane of the membrane) were scaled independently from z coordinates (perpendicular to the membrane), using the Parrinello-Rahman barostat.[72] The reference pressure was set to 1 bar and compressibility to 4.5×10^{-5} bar^{-1}. Short-range interactions were evaluated explicitly up to a cutoff of 1.0 nm and 1.2 nm for van der Waals and coulomb interactions, respectively. The shift algorithm was used for van der Waals interactions, and fast particle-mesh Ewald for long-range electrostatics, beyond these cut-off distances.[73] Explicit solvation was adopted for these simulations, using the TIP3P model for water.[66]

In the first step, the solvated membrane was equilibrated in the absence of ILs. After the initial membrane structure generated by CHARMM-GUI was relaxed with energy minimization, restraints were placed on the counter-ions by applying a force constant of 1000 kJ mol^{-1} nm^{-2} which were subsequently removed in the second part. The equilibration phase consisted of an initial MD simulation of 1 ns in the isochoric – isothermal ensemble (NVT) during which the temperature was gradually increased to 300 K. Subsequently, the membrane was equilibrated for 30 ns using the isobaric – isothermal ensemble (NPT).

In the next step, the IL ions were added to the solvated membrane. An initial energy minimization was followed by a 500 ps long NVT simulation with position restraints applied on phospholipids using a force constant of 1000 kJ mol^{-1} nm^{-2}. Subsequently, the restraints were

removed and an additional 500 ps long NVT simulation was performed. The entire system was then simulated for another 50 ns in the isobaric-isothermal ensemble (NPT). Lastly, an additional 40 ns NPT simulation was carried out with restraints applied on the z-coordinates of the cation ring atoms to allow equilibration of the membrane after cation insertions occurred in the previous phase. A harmonic potential with a force constant of 100 kJ mol^{-1} nm^{-2} was applied to these atoms. These restraints were necessary to prevent further cation insertion events. Data for analysis was averaged over 40 ns of the last NPT run, unless stated otherwise. Only the pure *E. coli*, i.e. the reference system, did not undergo the additional 40 ns NPT run since no cations in solution were present in that system. In that case, the last 10 ns of the NPT run were used for subsequent analysis.

3. Results and Discussion

3.1 Cation insertions

The extent of cation insertion was studied across different systems. Cation insertion in this case refers to those cations that diffuse into the bilayer, and remain inside it throughout the simulation. The amount of these cations that were transferred into the membrane is shown in Table 2.

Among the five systems shown in Table 2, varying degrees of cation insertion were observed indicating variations in cation absorption affinities, with noticeably more insertions of OMIM occurring than of OXMIM cations. This finding is in line with experimental findings, where the inclusion of a polar group in the cation alkyl chain indeed lowered toxicity and antimicrobial efficacy.[26,27] Furthermore, the observed cation insertions support the hypothesis that cations that contain long alkyl chains exhibit a stronger membrane affinity than those with shorter alkyl chains.[26] Moreover, when comparing the extent of insertion between ILs containing the same cation, it appears that those paired with lactate achieved more insertions, as compared to those with chloride. A possible reason for this observed anion effect is discussed in section 3.2.4.

TDMIM exhibits a different behavior as compared to the other cations during the simulations. Spontaneous formation of cation aggregates in water was observed within the first few nanoseconds of the simulations, independent of the identity of the anions, with a typical example shown in Figure 3. Aggregation started from only a few cations but grew rapidly. Eventually, an aggregate of 19 cations formed within 5 ns, with the only non-involved cation inserted into the bilayer. Subsequently, one more cation was transferred from the aggregate to the membrane. Aggregate formation can be attributed to the strong hydrophobic interactions due to the long aliphatic side chains and has already been frequently observed.[74-77] To avoid this aggregate formation, ion pairs in this system were only added gradually in several steps in subsequent simulations to keep the IL concentration in solution low at all times, as described in Section 2.3. Indeed, in these simulations all cations diffused into the membrane, which demonstrated the high membrane affinity of these cations. It will later be discussed by which factors cation insertion is influenced after a discussion of the insertion mechanism itself.

3.2 Local Characterization of Cation Insertion

3.2.1 Cation Insertion Mechanism

To investigate the extent and particulars of cation insertion, several of such insertion events were studied in greater detail, as shown in Figure 4. This was accomplished by determining the distance between the average value of the z-coordinate across all the phosphorus atoms in *each* leaflet and the centre-of-mass of the cation ring (head) and cation alkyl chain terminus (tail), respectively. This distance was calculated for the time window in which membrane insertion occurred. The plots in Figure 4 depict the progress of the cations as they approach and eventually penetrate the membrane, as revealed by the decreasing distance between the cation and the bilayer.

It was observed that before any cation insertion into or adsorption onto the membrane surface, the cation was oriented in such way that its alkyl tail pointed towards the membrane as indicated by the larger values of head – membrane distance as compared to tail – membrane

distance. This seemed somewhat unexpected, considering the non-polar properties of the alkyl chain and the strong polarity of the membrane surface. QM calculations have shown, however, that the positive charge is strongly delocalized over the entire cation including the alkyl chains (Fig. S1-S3 in Supporting Information). Similar results were also reported previously for the guanidinium family of cations.[74,78] A non-negligible electrostatic attraction between the cation tails and the negatively charged phospholipids would be the result. This interaction in combination, most importantly, with a reduced steric hindrance of the narrow alkyl chain compared to the more bulky ring, could explain the observed orientation of the tail.

The superimposition of the two curves in Figure 4 representing the distance of cation head and tail to the membrane layer, respectively, and the magnitude of their disparity also provide an insight into the orientation of the cation as they entered the membrane. A large difference between the curves indicates that the cation is oriented perpendicularly to the bilayer surface, while an overlapping set of curves suggests that the head and tail of the cation are oriented in parallel to the bilayer surface.

The plots in Figure 4 indicate that cation transfer into the membrane was always accompanied by a sharp drop in the distance between the tail and centre of bilayer (red curve in Figure 4). During the insertion, the cation tail typically remained closer to the membrane, relative to the head, indicating that the cations remained oriented with their tail pointing towards the membrane center. All plots in Figure 4 display a narrowing of the distance between the head and tail curves just before penetration occurs, which indicates that the cations were flatly adsorbed onto the membrane surface. Subsequently, the distance between head and tail increased again, with the tail – membrane centre distance decreasing rapidly while the head – membrane distance decreased only slightly. In other words, the cation alkyl chain penetrated the polar layer of the membrane with the lipid head groups and entered the hydrophobic part of the membrane. In the last step, the cation head and tail displayed a modest decrease in their respective distance relative to the membrane centre until a local equilibrium is reached where the head – tail distance remained constant. This suggests that the cations penetrated further into the membrane perpendicular to the membrane surface. Remarkable is that the adsorption

phase with the cations oriented in parallel to the membrane surface only lasted a few hundred picoseconds.

However, in Figure 4e, a somewhat different behavior was observed. In this plot, a 2 ns period existed in which the curves for cation head and tail overlapped before the actual insertion into the bilayer. This means that some of the larger TDMIM cations remained adsorbed on the membrane surface for about 2 ns until the alkyl chain fully extended itself into the hydrophobic core of the membrane. The longer adsorption time can be readily explained by considering that larger structural changes of the cation and the membrane are required until the larger cation can be accommodated by the membrane compared to smaller cations.

The schematic in Figure 5 illustrates the observed cation insertion mechanisms. Cations approach the membrane surface tail first, before being adsorbed for a short time onto the membrane surface, which leads to a cation orientation parallel to the surface. This step is then followed by cation insertion, where the cation briefly (about 200 ps) tilts at an angle relative to the membrane normal as it penetrates the membrane, followed by fully extending itself in parallel to the lipids once inside, as illustrated by steps 1, 2, 3a and 4 in Figure 5. The orientation in Step 3a has been commonly observed among the OMIM, OXMIM and TDMIM cations. Some TDMIM cations, however, adopted a slightly different orientation prior to penetration, by compacting their long alkyl tails during insertion and fully extending them once inserted. This mechanism is depicted in steps 1, 2, 3b and 4 in Figure 5. Anions did not seem to impact the insertion mechanism.

3.2.2 Structural Analysis of Local Environment around Cations

The centre-of-mass radial distribution functions (RDFs) were determined for several atom pairs across the various M_{EC} – IL systems. The number of groups N_i within a distance r of a specific group j was calculated by integrating the corresponding RDFs:

$$N_{ij} = 4\pi\rho_i \int_0^r g_{ij}(r') r'^2 dr' \qquad (2)$$

In eq 2, g_{ij} is the center-of-mass RDF of $i-j$ pairs, while ρ_i is the number density of compound i. The RDFs were integrated up to $r = r_{min}$, the position of the first minimum of the RDF to yield the average first coordination number of groups j around a group i.

The cations were categorized according to their positions during the simulation. Cations that diffused into the membrane and remained there are designated as *inserted* and the other cations as *non-inserted*. The coordination numbers were obtained individually for each cation according to Eq. 2, followed by averaging them according to whether they were inserted or non-inserted.

Coordination numbers of phosphorus atoms around the ring of an inserted cation in Table 3 show that within the first coordination sphere, between 1.3 to 1.4 phospholipids can be found around the cation. This small value was surprising as it implies that the inserted cation binds closely to just 1 to 2 lipid molecules. This finding is emphasized by the pronounced and narrow shape of the peak in Figure 6. This means that the cation – lipid head distance is well defined for all the systems surveyed and points to a strong cation – lipid interaction and strong ordering of the cations relative to the lipids.

Not surprisingly, the cations residing outside the membrane exhibited coordination numbers close to zero since they remained distant from the membrane throughout most of the simulations. The low values indicate that these cations remained well solvated in the bulk phase and were not adsorbed onto the membrane surface. The TDMIM-Lact system achieved 100% cation insertion, thereby leaving no cations outside for analysis. In general, there were no substantial differences found across systems.

The water distribution around the cations was also studied. Coordination numbers for water around cations show a marked difference between inserted and non-inserted cations, which is expected because the non-inserted cations remained fully solvated by water compared to inserted cations. However, although the inserted cations were mostly embedded into the membrane, the cation rings were aligned with the polar groups of the bilayer and exposed to the solvent. The values in Table 4 indicate that after penetrating the membrane, the cations

lost only approximately half of their solvation shell, indicating that hydration still plays an important role for cations post insertion. Another point to note is that among the inserted cations, those paired with chloride exhibited an increased degree of solvation. This is in agreement with weaker phospholipid – cation interactions for these systems, which will be discussed in section 3.2.4. A comparison of distances between cation head and bilayer center suggest that cations paired with lactate were inserted somewhat deeper into the bilayer, resulting in reduced solvation of these cations.

A diffusion of anions into the membrane was not observed in any simulation, even though anions regularly approached the surface due to attractive interactions with positively charged head groups of the phospholipids and the inserted cations.

3.2.3 Order Parameters of Cation Alkyl Chains

An order parameter study was performed to investigate the orientation of the alkyl chains contained in cations. Generally, order parameters are observables that can be obtained from experiments via deuterium NMR measurements and also through molecular simulations.[79] The order parameter S_{CD} is defined according to eq 3:

$$S_{CD} = \frac{3}{2} < cos^2\theta > -\frac{1}{2} \qquad (3)$$

For a saturated carbon chain, planes for each CH_2 group are defined in a way that all three atoms of that group lie in one of these planes. The angle θ is enclosed by vectors perpendicular to the planes of two consecutive CH_2 groups in the carbon chain. After averaging over all occurring orientations θ, the parameter S_{CD} can be obtained. Values of S_{CD} range from 0 to 1, where 0 is the case of lowest order, in which all possible angles of θ are found with the same probability, and 1 represents the highest order where all CH_2 groups are aligned in a straight line.

S_{CD} was determined for all cations in every system and are shown in Figure 7. For inserted cations, S_{CD} was averaged for individual cations only over those parts of the trajectory in which

the corresponding cation remained indeed inserted. These values were subsequently averaged over all inserted cations. A similar procedure was adopted for the non-inserted cations.

All five systems consistently showed a decreasing chain order with increasing distance from the imidazolium ring. Figure 7a for inserted cations also clearly shows the same trend of the curves for ILs that shared the same cations, thereby indicating that the choice of anion did not affect the orientation of the cation tails upon insertion. This was expected from the previous results, considering that anions did not pass the polar layer of the membrane. The order of non-inserted cation tails was generally close to zero, since no ordering in aqueous solution was to be expected, as shown in Figure 7b. Obtained values of S_{CD} for inserted cations were comparable with that of the phospholipids (see Section 3.3.3), indicating that the cations adopt a similar order as the lipids after insertion. This finding, combined with the preferred cation orientation discussed in Section 3.2.1 shows that inserted cations mimic the membrane lipids in terms of orientation and alkyl chain order.

The representative simulation snapshots in Figure 8 illustrate the flexibility of the alkyl chain tail of various cations in the membrane *post* insertion. While a linear orientation of the alkyl chain is commonly observed across all systems, disorder to a certain extent was still present. It can be seen from Figure 8a and 8b that for shorter cation tails, as in OMIM and OXMIM, the end of these alkyl chains exhibited a significant flexibility, as indicated by the decreasing S_{CD} values for carbons closer to the terminal methyl. On the other hand, the TDMIM cations remained mostly fully extended after insertion. These findings illustrate the results from the analysis of the order parameters that the TDMIM cations exhibited a larger S_{CD} value, i.e. larger order, than OMIM and OXMIM, as shown in Figure 7c. This differing behavior of cations consequently suggests that membrane properties are also affected differently, as will be discussed in later sections.

3.2.4 Analysis of Mutual Interactions of Ions and Membrane

Average interaction strengths, as well as their electrostatic and van der Waals contributions were determined between cations and anions, and between cations and the phosphate groups of phospholipids, respectively. Cations were divided into a group of inserted and non-inserted

cations as before. Interaction energies were obtained individually for every cation and averaged across all cations belonging to the same category, i.e. they represent the average interaction energy per cation with all other anions or lipid phosphates in the respective simulated system. The values for interaction strengths between cations and anions are shown in Table 5. Additionally, the centre-of-mass RDFs for pairs of anions and non-inserted cations as well as for pairs of membrane phosphorus atoms and anions are shown in Figures 9 and 10, respectively. Electrostatic and van der Waals contributions are labeled as E_{Coul} and E_{LJ}.

As expected, anions generally interacted more strongly with non-inserted cations than with inserted cations, due to the restricted solvent accessibility of the latter. Interactions of non-inserted cations and chloride were considerably stronger than with lactate. The RDFs of cation – anions pair distances in Figure 9 show a close coordination between cations and chloride as indicated by the strong peak at a distance of 4.2 Å. In contrast, a strong cation – anion coordination was not observed for lactate. As mentioned before, the strong cation – chloride coordination is a consequence of the strongly localized negative charge on these monoatomic ions. The strong coordination of chloride to OMIM and OXMIM could have been the underlying reason for the observed impeded cation insertion in these systems, because of the larger involved cation – anion dissociation energy that had to be overcome prior insertion.

After cation insertions occurred, we noticed an increased concentration of anions close to the membrane surface in the system that involved OMIM-Lact, as shown in Figure 10. This increased local anion concentration was indeed also accompanied by an increased interaction strength of inserted OMIM with lactate anions, compared to all other systems. The largest number of inserted cations was observed in the same system, which simply means that the increased positive membrane surface charge attracted more anions from the solvent. A similar trend, albeit weaker, was observed for OXMIM-Lact compared to OXMIM-Cl. However, such a trend was not observed for OMIM-Cl compared to OXMIM-Cl. Even though substantially more insertions of OMIM compared to OXMIM were observed, the chloride concentration in systems involving OMIM did not increase at the membrane surface. Due to the possibility of forming a

strong cation – chloride coordination in these systems, it appears that chloride preferred to maintain its coordination with non-inserted and thereby more accessible cations.

Average interaction strengths of inserted cations with phosphate groups of lipids are shown in Table 6. Strong electrostatic attraction between these inserted cations and phosphates was found, which was of comparable magnitude as those between non-inserted cations and anions. That means that cation insertion is facilitated by compensating energetically unfavorable cation – anion dissociation and partial cation dehydration not only by an obvious hydrophobic effect, in which the non-polar cation alkyl chain is transferred from polar water to the hydrophobic core of the membrane but also by electrostatic attraction between the positively charged imidazolium ring and negatively charged phosphate.

Furthermore, a trend connecting weak hydration of inserted cations, as shown in Table 4, and strong cation – phosphate interactions was found. As discussed previously, weaker hydration was found for OXMIM compared to OMIM and for lactate compared to chloride. Also, inserted TDMIM exhibited weak hydration together with the strongest interaction with the phosphates. The decreased hydration, i.e. reduced solvent accessibility, of the inserted cation together with stronger interactions with the lipid phosphates is indicative of a deeper insertion of the cation into the membrane. This is clearly demonstrated for instance in Figure 8, where a deeper penetration of OXMIM compared to OMIM is illustrated. This behavior was caused by the negatively charged oxygen in the alkyl chain of OXMIM. Unfavorable interactions with the also negatively charged phosphates in its vicinity led to a repellant force that pushed the cation deeper into the membrane to increase the distance between the oxygen and neighboring phosphates. Overcoming this additional repulsive interaction might have caused the observed impeded cation insertion of OXMIM compared to OMIM.

3.3 Non-local Membrane Changes Induced by ILs

3.3.1 Changes in Membrane Surface Density and Thickness

The surface area of the membrane was evaluated before and after cation insertions to determine the extent of disruption. The surface area of the membrane was divided by the number of molecules in each leaflet. Molecules here refer to the total number of phospholipids and inserted cations present in the leaflet after completion of the unrestrained simulations.

A decrease in the surface area per molecule compared to the *E. coli* membrane without ILs was observed in all systems, with the exception of the OXMIM-Cl system. The results are shown in Table 7. The surface area per molecule is a measure of how tightly packed molecules are in the membrane. Its value depends on several factors, such as interaction strength between neighboring molecules in a leaflet, hydration of the membrane surface, thickness of the bilayer and size of inserted cations.

The area per molecule tended to decrease upon cation insertion because cations in contrast to lipids contain only one alkyl chain and thus displace fewer lipids compared to the insertion of an additional lipid. This effect was particularly pronounced in the case of TDMIM insertion. The TDMIM cations were oriented in parallel to the phospholipids with a reduced tendency to curl as indicated by larger order parameters as shown in Figure 7c and also illustrated in Figure 8c. However, OMIM and OXMIM cations showed a tendency to slant and curl, which led to an occupation of a larger amount of space within the membrane. This in turn caused an increase in surface area and a larger area per molecule compared to TDMIM, as shown in Figures 8a and 8b.

Thickness of the membrane was obtained by measuring the distance between the average z-coordinate of the phosphorus atoms in each leaflet. In X-ray diffraction experiments, the membrane thickness can be measured as the distance between the two maxima of the electron density profile, which correspond to the average positions of the electron rich phosphates.[54]

All systems showed a reduction in membrane thickness by 0.2 - 0.3 nm as compared to the membrane without IL, except for the case of TDMIM-Lact, as shown in Table 7. When cations

with shorter alkyl chains, i.e. OMIM and OXMIM, were inserted into the membrane, local voids were formed within the hydrophobic core of the bilayer. This was caused by the cation tails that were shorter than the fatty acids of the phospholipids, which in turn enabled the long tails of the phospholipids to curl and bend into these generated voids. This effectively reduced the average expansion of the lipids in the direction perpendicular to the membrane surface, thus reducing the membrane thickness. In the case of TDMIM-Lact, the TDMIM cation contained a 14-carbon long alkyl chain, which is of comparable length as the phospholipid fatty acids. As a result, upon insertion into the membrane, less empty space was created between the lipids as compared to OMIM and OXMIM insertions, resulting in a thickness that was close to the IL-free reference membrane.

Roughness of the membrane surface, r_{m}, was determined by calculating the average deviation of the z-coordinates of phosphorus atoms in each leaflet of the bilayer from the membrane surface, as shown in eq 4:

$$r_m = \frac{1}{n}\sum_i |z_i - \bar{z}| \qquad (4)$$

The average z-coordinate of all phosphorus atoms in one leaflet is designated as $\bar{z}$, while z_i denotes the z-coordinate of each individual phosphorus atom. The number of phospholipids in a leaflet is represented by n. Values were averaged over the length of the trajectory. The roughness provides some insight into the arrangement of the phospholipids and whether the membrane surface is smooth or disordered.

The results are listed in Table 7. No statistically significant changes in roughness could be observed after cation insertions. Only in the case of TDMIM, the roughness value was slightly reduced, suggesting an ordering effect on phospholipids induced by TDMIM. On the whole, cation insertions did not seem to substantially alter the membrane surface. The influence of cation insertions on the hydrophobic membrane core will be examined further in subsequent sections.

3.3.2 Membrane Electron Density Profiles

The density profiles shown in Figure 11 represent the electron density in the direction perpendicular to the membrane surface. In that direction, the bilayer was divided into 100 equally sized slices. The electron density for each slice was then obtained by summing the number of electrons within that slice and subsequent averaging over all structures. Such density profiles can provide information regarding membrane order, thickness and overall distribution of the membrane components.

Density profiles of the membranes that contained lactate were superimposed with that of the IL-free membrane. Two distinct peaks can be seen for each curve that correspond to the positions of the phosphate layers that delimit the hydrophobic part of the membrane. The distance between these peaks defines the membrane thickness. The peak widths correspond to the roughness of the membrane surface. Figure 11 shows that the electron density for the IL-free reference membrane is larger than for all other systems, except for the innermost region of the bilayer where z = 0 nm. These differences, however, are less pronounced for the TDMIM-Lact system. The reduced densities observed around z = ±1 nm for all bilayer – IL systems as compared to the IL-free membrane can be attributed to voids that were generated upon cation insertion, as mentioned in the previous section. This led to an increase in lipid disorder, which will be discussed in the next section. Electron densities in the bilayer – water interface were also found to be smaller compared to the IL-free membrane. In contrast to phospholipids that expose head groups to the solvent, inserted cations did not extend far into the solvent, which caused the disappearance of the peak shoulder in direction of the solvent. Lastly, at the innermost regions of the bilayer, most systems displayed a larger density than in the IL-free membrane. This can be attributed to the thinning of these membranes after cation insertions, whereby both leaflets approached each other, as discussed in the previous section. Such an approach of opposing leaflets resulted in a higher density at the centre of the bilayer.

Qualitatively similar effects were observed also for systems containing chloride, however, these effects were less pronounced due to the smaller number of cation insertions. Hence, corresponding plots were omitted.

3.3.3 Order Parameters of Phospholipid Fatty Acids

In this section, the chain order parameters according to eq 3 were determined for the fatty acids contained in phospholipids, in order to examine the effects of cation insertion on phospholipid behavior. The *E. coli* membrane model is composed of three different phospholipids. For this analysis, however, only the most prevalent POPE lipid was chosen. Each phospholipid contained an oleoyl and a palmitoyl tail. Their respective order parameters are shown in Figures 12a and 12b.

Ordering of the two kinds of fatty acids exhibited distinct characteristics, which were qualitatively similar in all systems. For instance, oleoyl showed increased order between the carbons C9 and C11, in contrast to palmitoyl. This section of the oleoyl chain corresponds to the atoms in the vicinity of the cis double bond. As expected, a general tendency of increasing disorder closer to the termini of the fatty acids was observed. Overall, these order characteristics were typical for these types of fatty acids and have been observed on numerous occasions before.

From Figure 12 it is possible to observe that cation insertions caused a disordering of the phospholipid side chains relative to those in the IL-free membrane. OMIM and OXMIM systems involved cations which were more slanted and bent within the bilayer due to their limited alkyl chain length, as illustrated in Figures 8a and 8b. Moreover, the data shown in Figure 12 demonstrates that cation insertions into the bilayer that contained OMIM-Lact induced the largest disordering effect with respect to the IL-free membrane. Most cation insertions were also observed in this system. On the contrary, the membrane system that contained TDMIM-Lact, however, displayed an increased ordering of the phospholipids. As already suggested by previous results, TDMIM alkyl chains were of similar length as fatty acids, as shown for instance in Figure 8c, thereby causing only minimal perturbation of the membrane.

For the TDMIM-Lact system, the lipid order parameters were studied in greater detail. POPE lipids were assigned to two different groups, where one group contained all lipids within 0.5 nm

of the inserted cation and the second group all others. The aim was to see whether there is a relationship between phospholipid order and its proximity to the inserted cation. The results are shown in Figure 13. It was found that phospholipids located within 0.5 nm of inserted cations were indeed more ordered than those that were not within the immediate environment of an inserted cation. Overall, the results indicate that cations with long alkyl chains appear to mimic the behavior of the lipid molecules, a phenomenon that has also been observed in experiments.[37,80] This induced ordering effect, however, fades as the distance between phospholipid and inserted cation increased. This means that the average ordering effect observed before due to TDMIM insertions was a consequence of local lipid ordering but not due to an overall ordering of the entire membrane. The order parameter analysis was also repeated for POPG, where the same results were obtained.

4. Conclusion

In this work we investigated the insertions of imidazolium-based cations from different ILs into a phospholipid bilayer which thereby induced structural changes. The membrane model was based on the plasma membrane of *E. coli*. Cation insertions to varying extents were observed for all considered ILs. Substantially more insertions of OMIM than of OXMIM occurred, while the presence of chloride led to fewer cation insertions compared to lactate. Impeded OXMIM insertion appeared to have been caused by the necessity of overcoming the repulsion between the negatively charged oxygen in the cation alkyl chain and the negatively charged lipid phosphate. Reduced antimicrobial activity of similarly functionalized cations has been observed before. Furthermore, chloride coordinated more favorably with cations than lactate, so that cations were required to overcome a larger average anion dissociation energy to enable insertion into the membrane, thus impeding the process.

Cations inserted with their alkyl tail first into the membrane. In the case of OMIM and OXMIM, only very short periods of a few 100 ps were observed in which the cation remained temporarily adsorbed on the membrane surface with an orientation parallel to the surface. The adsorption phase was in some cases of TDMIM insertion extended due to more extensive

membrane reorganization, which was necessary in order to accommodate these larger cations. Furthermore, OXMIM head groups penetrated somewhat deeper into the membrane than OMIM and TDMIM, due to electrostatic repulsion between the negatively charged oxygen in the alkyl chain and negatively charged lipid phosphates. As a result, OXMIM remained less solvated after insertion.

Once inserted into the membrane, strong electrostatic interactions between the cation and adjacent phospholipids led to an association of the cation within a well-defined distance to only one or two lipids. After insertion, about half of the hydration shell of the cations was maintained due to the partial exposure of the imidazolium ring to the solvent. Hence, cations remained susceptible to the presence of anions in the solvent to some extent, which influenced cation – membrane interactions notably but not substantially. Overall, membrane properties were influenced primarily by the IL cations. Moreover, anions did not adsorb onto the membrane surface for prolonged periods of time nor diffuse into the membrane.

After insertion, cation tails were oriented in parallel to the membrane lipids with an overall alkyl chain ordering similar to those of fatty acids in the membrane. The alkyl tail of TDMIM, which is of similar length compared to neighboring lipids, was particularly ordered, i.e. maintained a straight conformation perpendicular to the membrane surface. The alkyl ends of the shorter tails of OMIM and OXMIM, however, were more flexible and tended to curl. Furthermore, lipids in the membrane were found to be less ordered after insertions of OXMIM and OMIM. On the contrary, after insertion of TDMIM, the order of adjacent lipids increased locally.

Membrane properties clearly changed after cation insertions. The average membrane surface area per molecule decreased due to the smaller size of the cations compared to lipids. The short alkyl tails of OMIM and OXMIM generated voids in the hydrophobic part of the bilayer that in turn led to increased disorder of the lipids to fill these voids by curling their fatty acid tails. The less ordered fatty acids caused the two bilayers to move closer together, thereby reducing the membrane thickness. This effect was not observed after TDMIM insertions

because the longer cation alkyl chain prevented void formation in the bilayer. The surface roughness of the membrane was not increased by cation insertions.

Overall, the results suggest that mostly cations affect cell membranes, while anions only play a secondary role in accordance with experimental observations. Smaller cations such as OMIM and OXMIM changed membrane properties considerably due to their mismatch in length compared to lipids. It is reasonable to assume that significant changes in membrane properties are disadvantageous compared to an unaffected cell to function normally, thereby suggesting the possibility of antimicrobial activity and toxicity of these cations. Larger TDMIM barely changed membrane properties due to their similarity to lipids. However, this also indicates that these cations exhibit a higher affinity for membrane insertions than OMIM and OXMIM, which was indeed indicated by our simulations. This would lead to a stronger accumulation of cations in the membrane over time, which would strongly affect the membrane on a time scale that was not accessible with applied simulation techniques. Due to the negative surface charge of the bacterial membrane surface, a direct contact with solvated imidazolium cations is inevitable. Once in contact with the bacterial surface, cations will most likely interact with phospholipids, which dominantly contribute to the composition of the membrane. Therefore, the considered system consisting of a phospholipid bilayer in contact with solvated cations is an adequate description to study non-specific antimicrobial effects induced by cations, even though the bilayer model considered here is of a smaller scale and lacks some of the components found in actual bacterial membranes. Possible specific antimicrobial effects caused by interactions of cations with other membrane components, such as e.g. transmembrane proteins, were beyond the scope of this work. The next step for future work will be to study quantitatively the partitioning of different cations into membranes as well as the long-term effect of cation insertions on membrane properties. The present work demonstrates how MD simulations can be used to study the impact of diluted ILs on membranes with high structural and energetic detail and how these influences on the membrane are connected with single basic structural features of the involved ions.

Supporting Information

Atom names, atom types and charges for the considered cations and anions (Table S1), and partial charges of all considered cations and anions solvated in water used for the force field parameterization (Figures S1 – S4) are given. This material is available free of charge via the internet at http://pubs.acs.org.

Acknowledgments

We gratefully acknowledge the provision of computational facilities by the A*STAR Computational Resource Centre of Singapore (ACRC) and the Institute of High Performance Computing (IHPC) as well as the financial support from the Joint Council Office (JCO) of the Agency for Science, Technology and Research (A*STAR) of Singapore**.**

References

(1) Who | World Health Day - 7 April 2011. http://www.who.int/world-health-day/2011/en/ Accessed on 28 April 2014

(2) Hancock, R. E. W.; Lehrer, R. Cationic Peptides: A New Source of Antibiotics. *Trends Biotechnol.* **1998**, *16*, 82-88

(3) Zasloff, M. Antimicrobial Peptides of Multicellular Organisms. *Nature* **2002**, *415*, 389-395.

(4) Seo, M.-D.; Won, H.-S.; Kim, J.-H.; Mishig-Ochir, T.; Lee, B.-J. Antimicrobial Peptides for Therapeutic Applications: A Review. *Molecules* **2012**, *17*, 12276-12286.

(5) Fox, J. L. Antimicrobial Peptides Stage a Comeback. *Nat. Biotechnol.* **2013**, *31*, 379-382.

(6) Giuliani, A.; Pirri, G.; Nicoletto, S. F. Antimicrobial Peptides: An Overview of a Promising Class of Therapeutics. *Cent. Eur. J. Biol.* **2007**, *2*, 1–33.

(7) Brogden, K. A. Antimicrobial Peptides: Pore Formers or Metabolic Inhibitors in Bacteria? *Nature Rev. Microbiol.* **2005**, *3*, 238-250.

(8) Nederberg, F.; Zhang, Y.; Tan, J. P. K.; Xu, K.; Wang, H.; Yang, C.; Gao, S.; Guo, X. D.; Fukushima, K.; Li, L. *et al.* Biodegradable Nanostructures with Selective Lysis of Microbial Membranes. *Nat. Chem.* **2011**, *3*, 409-414.

(9) Hancock, R. E. W.; Sahl, H.-G. Antimicrobial and Host-Defense Peptides as New Anti-Infective Therapeutic Strategies. *Nat. Biotechnol.* **2006**, *24*, 1551-1557.

(10) Patch, J. A.; Barron, A. E. Mimicry of Bioactive Peptides Via Non-Natural, Sequence-Specific Peptidomimetic Oligomers. *Curr. Opin. Chem. Biol.* **2002**, *6*, 872–877.

(11) Rotem, S.; Mor, A. Antimicrobial Peptide Mimics for Improved Therapeutic Properties. *Biochim. Biophys. Acta* **2009**, *1788*, 1582–1592.

(12) Gilmore, B. F. Antimicrobial Ionic Liquids. In *Ionic Liquids: Applications and Perspectives*; Kokorin, P. A., Ed.; InTech, 2011; pp 587-604.
(13) Welton, T. Room-Temperature Ionic Liquids. Solvents for Synthesis and Catalysis. *Chem. Rev.* **1999**, *99*, 2071-2084.
(14) Rogers, R. D.; Seddon, K. R. Ionic Liquids - Solvents of the Future? *Science* **2003**, *302*, 792-793.
(15) Weingärtner, H. Understanding Ionic Liquids at the Molecular Level: Facts, Problems, and Controversies. *Angew. Chem. Int. Ed.* **2008**, *47*, 654-670.
(16) Tokuda, H.; Hayamizu, K.; Ishii, K.; Abu Bin Hasan Susan, M.; Watanabe, M. Physicochemical Properties and Structures of Room Temperature Ionic Liquids. 1. Variation of Anionic Species. *J. Phys. Chem. B* **2004**, *108*, 16593-16600.
(17) Tokuda, H.; Hayamizu, K.; Ishii, K.; Susan, M.; Watanabe, M. Physicochemical Properties and Structures of Room Temperature Ionic Liquids. 2. Variation of Alkyl Chain Length in Imidazolium Cation. *J. Phys. Chem. B* **2005**, *109*, 6103-6110.
(18) Tokuda, H.; Ishii, K.; Susan, M.; Tsuzuki, S.; Hayamizu, K.; Watanabe, M. Physicochemical Properties and Structures of Room-Temperature Ionic Liquids. 3. Variation of Cationic Structures. *J. Phys. Chem. B* **2006**, *110*, 2833-2839.
(19) Petkovic, M.; Seddon, K. R.; Rebelo, L. P. N.; Pereira, C. S. Ionic Liquids: A Pathway to Environmental Acceptability. *Chem. Soc. Rev.* **2011**, *40*, 1383-1403.
(20) Pham, T. P. T.; Cho, C.-W.; Yun, Y.-S. Environmental Fate and Toxicity of Ionic Liquids: A Review. *Water Res.* **2010**, *44*, 352-372.
(21) Romero, A.; Santos, A.; Tojo, J.; Rodríguez, A. Toxicity and Biodegradability of Imidazolium Ionic Liquids. *J. Hazard. Mater.* **2008**, *151*, 268-273.
(22) Zhao, D.; Wu, M.; Kou, Y.; Min, E. Ionic Liquids: Applications in Catalysis. *Catal. Today* **2002**, *74* 157–189.
(23) Olivier-Bourbigou, H.; Magna, L. Ionic Liquids: Perspectives for Organic and Catalytic Reactions. *J. Mol. Catal. A: Chem.* **2002**, *182*, 419-437.
(24) Pernak, J.; Goc, I.; Mirska, I. Anti-Microbial Activities of Protic Ionic Liquids with Lactate Anion. *Green Chem.* **2004**, *6*, 323-329.
(25) Zhao, D. B.; Liao, Y. C.; Zhang, Z. D. Toxicity of Ionic Liquids. *CLEAN* **2007**, *35*, 42-48.
(26) Stolte, S.; Matzke, M.; Arning, J.; Böschen, A.; Pitner, W.-R.; Welz-Biermann, U.; Jastorff, B.; Ranke, J. Effects of Different Head Groups and Functionalised Side Chains on the Aquatic Toxicity of Ionic Liquids. *Green Chem.* **2007**, *9*, 1170–1179.
(27) Morrissey, S.; Pegot, B.; Coleman, D.; Garcia, M. T.; Ferguson, D.; Quilty, B.; Gathergood, N. Biodegradable, Non-Bactericidal Oxygen-Functionalised Imidazolium Esters: A Step Towards 'Greener' Ionic Liquids. *Green Chem.* **2009**, *11*, 475–483.
(28) Coleman, D.; Špulák, M.; Garcia, M. T.; Gathergood, N. Antimicrobial Toxicity Studies of Ionic Liquids Leading to a 'Hit' Mrsa Selective Antibacterial Imidazolium Salt. *Green Chem.* **2012**, *14*, 1350-1356.
(29) Gathergood, N.; Garcia, M. T.; Scammells, P. J. Biodegradable Ionic Liquids: Part I. Concept, Preliminary Targets and Evaluation. *Green Chem.* **2004**, *6*, 166-175.
(30) Pfruender, H.; Jones, R.; Weuster-Botz, D. Water Immiscible Ionic Liquids as Solvents for Whole Cell Biocatalysis. *J. Biotechnol.* **2006**, *124*, 182–190.
(31) Wasserscheid, P.; Welton, T. *Ionic Liquids in Synthesis*, 2 ed.; Wiley-VCH Verlag GmbH & Co. KGaA: Weinheim 2008; Vol. 1.
(32) Pernak, J.; Sobaszkiewicz, K.; Mirska, I. Anti-Microbial Activities of Ionic Liquids. *Green Chem.* **2003**, *5*, 52–56.

(33) Demberelnyamba, D.; Kim, K.-S.; Choi, S.; Park, S.-Y.; Lee, H.; Kim, C.-J.; Yoo, I.-D. Synthesis and Antimicrobial Properties of Imidazolium and Pyrrolidinonium Salts. *Bioorg. Med. Chem.* **2004**, *12*, 853–857.
(34) Docherty, K. M.; Charles F. Kulpa, J. Toxicity and Antimicrobial Activity of Imidazolium and Pyridinium Ionic Liquids. *Green Chem.* **2005**, *7*, 185–189.
(35) Salminen, J.; Papaiconomou, N.; Kumar, R. A.; Lee, J.-M.; Kerr, J.; Newman, J.; Prausnitz, J. M. Physicochemical Properties and Toxicities of Hydrophobic Piperidinium and Pyrrolidinium Ionic Liquids. *Fluid Phase Equilib.* **2007**, *261*, 421–426.
(36) Cornellas, A.; Perez, L.; Comelles, F.; Ribosa, I.; Manresa, A.; Garcia, M. T. Self-Aggregation and Antimicrobial Activity of Imidazolium and Pyridinium Based Ionic Liquids in Aqueous Solution. *J. Colloid Interface Sci.* **2011**, *355* 164–171.
(37) Łuczak, J.; Jungnickel, C.; Łacka, I.; Stolte, S.; Hupka, J. Antimicrobial and Surface Activity of 1-Alkyl-3-Methylimidazolium Derivatives. *Green Chem.* **2010**, *12*, 593–601.
(38) Carson, L.; Chau, P. K. W.; Earle, M. J.; Gilea, M. A.; Gilmore, B. F.; Gorman, S. P.; McCann, M. T.; Seddon, K. R. Antibiofilm Activities of 1-Alkyl-3-Methylimidazolium Chloride Ionic Liquids. *Green Chem.* **2009**, *11*, 492–497.
(39) Cromie, S. R. T.; Pópolo, M. G. D.; Ballone, P. Interaction of Room Temperature Ionic Liquid Solutions with a Cholesterol Bilayer. *J. Phys. Chem. B* **2009**, *113*, 11642–11648.
(40) Bingham, R. J.; Ballone, P. Computational Study of Room-Temperature Ionic Liquids Interacting with a Popc Phospholipid Bilayer. *J. Phys. Chem. B* **2012**, *116*, 11205–11216.
(41) Klähn, M.; Zacharias, M. Transformations in Plasma Membranes of Cancerous Cells and Resulting Consequences for Cation Insertion Studied with Molecular Dynamics. *Phys. Chem. Chem. Phys.* **2013**, *15*, 14427-14441.
(42) Kumar, V.; Malhotra, S. V. Study on the Potential Anti-Cancer Activity of Phosphonium and Ammonium-Based Ionic Liquids. *Bioorg. Med. Chem. Lett.* **2009**, *19*, 4643–4646.
(43) Ranke, J.; Mölter, K.; Stock, F.; Bottin-Weber, U.; Poczobutt, J.; Hoffmann, J.; Ondruschka, B.; Filser, J.; Jastorff, B. Biological Effects of Imidazolium Ionic Liquids with Varying Chain Lengths in Acute Vibrio Fischeri and Wst-1 Cell Viability Assays. *Ecotoxicol. Environ. Saf.* **2004**, *58*, 396–404.
(44) Vanommeslaeghe, K.; Hatcher, E.; Acharya, C.; Kundu, S.; Zhong, S.; Shim, J.; Darian, E.; Guvench, O.; Lopes, P.; Vorobyov, I. *et al.* Charmm General Force Field: A Force Field for Drug-Like Molecules Compatible with the Charmm All-Atom Additive Biological Force Fields. *J. Comput. Chem.* **2010**, *31*, 671-690.
(45) Vanommeslaeghe, K.; MacKerell Jr., A. D. Automation of the Charmm General Force Field (Cgenff) I: Bond Perception and Atom Typing. *J. Chem. Inf. Model.* **2012**, *52*, 3144-3154.
(46) Vanommeslaeghe, K.; Raman, E. P.; MacKerell Jr., A. D. Automation of the Charmm General Force Field (Cgenff) Ii: Assignment of Bonded Parameters and Partial Atomic Charges. *J. Chem. Inf. Model.* **2012**, *52*, 3155-3168.
(47) Besler, B. H.; Kenneth M. Merz, J.; Kollman, P. A. Atomic Charges Derived from Semiempirical Methods. *J. Comput. Chem.* **1990**, *11*, 431-439.
(48) Singh, U. C.; Kollman, P. A. An Approach to Computing Electrostatic Charges for Molecules. *J. Comput. Chem.* **1984**, *5*, 129-145.
(49) Frisch, M. J.; Trucks, G. W.; Schlegel, H. B.; Scuseria, G. E.; Robb, M. A.; Cheeseman, J. R.; Scalmani, G.; Barone, V.; Mennucci, B.; Petersson, G. A. *et al.* Gaussian 09, Revision D.01, Gaussian, Inc. ; Wallingford CT, 2009, 2009.
(50) Tomasi, J.; Mennucci, B.; Cammi, R. Quantum Mechanical Continuum Solvation Models. *Chem. Rev.* **2005**, *105*, 2999-3093.

(51) Palomar, J.; Ferro, V. R.; Torrecilla, J. S.; Rodríguez, F. Density and Molar Volume Predictions Using Cosmo-Rs for Ionic Liquids. An Approach to Solvent Design. *Ind. Eng. Chem. Res.* **2007**, *46*, 6041-6048.
(52) Wang, J.-y.; Jiang, H.-c.; Liu, Y.-m.; Hu, Y.-q. Density and Surface Tension of Pure 1-Ethyl-3-Methylimidazolium L-Lactate Ionic Liquid and Its Binary Mixtures with Water. *J. Chem. Thermodynamics* **2011**, *43* 800–804.
(53) Epand, R. F.; Schmitt, M. A.; Gellman, S. H.; Epand, R. M. Role of Membrane Lipids in the Mechanism of Bacterial Species Selective Toxicity by Two A/B-Antimicrobial Peptides. *Biochim. Biophys. Acta* **2006**, *1758*, 1343–1350.
(54) Yeagle, P. L. *The Membranes of Cells*, 2nd ed.; Academic Press, 1993.
(55) Snyder, D. S.; McIntosh, T. J. The Lipopolysaccharide Barrier: Correlation of Antibiotic Susceptibility with Antibiotic Permeability and Fluorescent Probe Binding Kinetics. *Biochemistry* **2000**, *39*, 11777-11787.
(56) Jo, S.; Kim, T.; Im, W. Automated Builder and Database of Protein/Membrane Complexes for Molecular Dynamics Simulations. *Plos One* **2007**, *2*.
(57) Jo, S.; Kim, T.; Iyer, V. G.; Im, W. Charmm-Gui: A Web-Based Graphical User Interface for Charmm. *J. Comput. Chem.* **2008**, *29*, 1859-1865.
(58) Jo, S.; Lim, J. B.; Klauda, J. B.; Im, W. Charmm-Gui Membrane Builder for Mixed Bilayers and Its Application to Yeast Membranes. *Biophys. J.* **2009**, *97*, 50-58.
(59) Woolf, T. B.; Roux, B. Molecular-Dynamics Simulation of the Gramicidin Channel in a Phospholipid-Bilayer. *Proc. Natl. Acad. Sci. U.S.A.* **1994**, *91*, 11631-11635.
(60) Hyvonen, M. T.; Kovanen, P. T. Molecular Dynamics Simulations of Unsaturated Lipid Bilayers: Effects of Varying the Numbers of Double Bonds. *Eur. Biophys. J. Biophy.* **2005**, *34*, 294-305.
(61) Janosi, L.; Gorfe, A. A. Simulating Popc and Popc/Popg Bilayers: Conserved Packing and Altered Surface Reactivity. *J. Chem. Theory Comput.*, *6*, 3267-3273.
(62) Klauda, J. B.; Venable, R. M.; Freites, J. A.; O'Connor, J. W.; Tobias, D. J.; Mondragon-Ramirez, C.; Vorobyov, I.; MacKerell Jr., A. D.; Pastor, R. W. Update of the Charmm All-Atom Additive Force Field for Lipids: Validation on Six Lipid Types. *J. Phys. Chem. B* **2010**, *114*, 7830-7843.
(63) Piggot, T. J.; Piñeiro, Á.; Khalid, S. Molecular Dynamics Simulations of Phosphatidylcholine Membranes: A Comparative Force Field Study. *J. Chem. Theory Comput.* **2012**, *8*, 4593–4609.
(64) Zidar, J.; Merzel, F.; Hodošček, M.; Rebolj, K.; Sepčić, K.; Maček, P.; Janežič, D. Liquid-Ordered Phase Formation in Cholesterol/Sphingomyelin Bilayers: All-Atom Molecular Dynamics Simulations. *J. Phys. Chem. B* **2009**, *113*, 15795–15802.
(65) Pastor, R. W.; MacKerell Jr., A. D. Development of the Charmm Force Field for Lipids. *J. Phys. Chem. Lett.* **2011**, *2*, 1526-1532.
(66) Jorgensen, W. L.; Chandrasekhar, J.; Madura, J. D.; Impey, R. W.; Klein, M. L. Comparison of Simple Potential Functions for Simulating Liquid Water. *J. Chem. Phys.* **1983**, *79*, 926-935.
(67) van der Spoel, D.; Lindahl, E.; Hess, B.; Groenhof, G.; Mark, A. E.; Berendsen, H. J. C. Gromacs: Fast, Flexible, and Free. *J. Comput. Chem.* **2005**, *26*, 1701-1718.
(68) Hess, B.; Kutzner, C.; van der Spoel, D.; Lindahl, E. Gromacs 4: Algorithms for Highly Efficient, Load-Balanced, and Scalable Molecular Simulation. *J. Chem. Theory Comput.* **2008**, *4*, 435-447.
(69) Hess, B.; Bekker, H.; Berendsen, H. J. C.; Fraaije, J. Lincs: A Linear Constraint Solver for Molecular Simulations. *J. Comput. Chem.* **1997**, *18*, 1463-1472.
(70) Hoover, W. G. Canonical Dynamics - Equilibrium Phase-Space Distributions. *Phys. Rev. A* **1985**, *31*, 1695-1697.
(71) Nose, S. A Unified Formulation of the Constant Temperature Molecular-Dynamics Methods. *J. Chem. Phys.* **1984**, *81*, 511-519.

(72) Parrinello, M.; Rahman, A. Polymorphic Transitions in Single-Crystals - a New Molecular-Dynamics Method. *J. Appl. Phys.* **1981**, *52*, 7182-7190.
(73) Darden, T.; York, D.; Pedersen, L. Particle Mesh Ewald - an N.Log(N) Method for Ewald Sums in Large Systems. *J. Chem. Phys.* **1993**, *98*, 10089-10092.
(74) Seduraman, A.; Klähn, M.; Wu, P. Characterization of Nano-Domains in Ionic Liquids with Molecular Simulations. *Calphad* **2009**, *33*, 605-613.
(75) Bhargava, B. L.; Klein, M. L. Molecular Dynamics Studies of Cation Aggregation in the Room Temperature Ionic Liquid [C10mim][Br] in Aqueous Solution. *J. Phys. Chem. A* **2009**, *113*, 1898–1904.
(76) Jiang, W.; Wang, Y.; Voth, G. A. Molecular Dynamics Simulation of Nanostructural Organization in Ionic Liquid/Water Mixtures. *J. Phys. Chem. B* **2007**, *111*, 4812-4818.
(77) Lopes, J. N. A. C.; Pádua, A. A. H. Nanostructural Organization in Ionic Liquids. *J. Phys. Chem. B* **2006**, *110*, 3330-3335.
(78) Klähn, M.; Seduraman, A.; Wu, P. A Force Field for Guanidinium-Based Ionic Liquids That Utilizes the Electron Charge Distribution of the Actual Liquid: A Molecular Simulation Study. *J. Phys. Chem. B* **2008**, *112*, 10989-11004.
(79) Vermeer, L. S.; Groot, B. L. d.; Réat, V.; Milon, A.; Czaplicki, J. Acyl Chain Order Parameter Profiles in Phospholipid Bilayers: Computation from Molecular Dynamics Simulations and Comparison with 2h Nmr Experiments. *Eur Biophys J* **2007**, *36*, 919–931.
(80) Birnie, C. R.; Malamud, D.; Schnaare, R. L. Antimicrobial Evaluation of N-Alkyl Betaines and N-Alkyl-N,N-Dimethylamine Oxides with Variations in Chain Length. *Antimicrob. Agents Chemother.* **2000**, *44*, 2514–2517.

Table 1: Composition of Membrane and its Solvent with ILs

Membrane	N_{lipids}[a]		
POPE	32		
POPG	6		
POPA	2		
Added IL	$N_{ion\text{-}pairs}$	N_{water}	N_{atoms}
OMIM-Lact	20	4414	24206
OMIM-Cl	20	4473	24183
OXMIM-Lact	20	4333	24043
OXMIM-Cl	20	4418	24098
TDMIM-Lact	6	4320	23360
Pure *E. coli.*[b]	0	4813	24443

[a] Number of phospholipids per layer.

[b] This system only contained the solvated *E. coli* membrane without IL as the reference model.

Table 2: Amount of Cation Insertions in Different IL – Membrane Systems

IL	N_{insert}[a]
OMIM-Lact	14(0.7)
OMIM-Cl	10(0.5)
OXMIM-Lact	10(0.5)
OXMIM-Cl	6(0.3)
TDMIM-Lact	6(1.0)

[a] Number of cations that were inserted during simulations, with the corresponding cation fraction in parenthesis.

Table 3: **Number of Membrane Lipids Coordinated to Cations**[a]

IL	Inserted Cations $N_{cat\text{-}lip}$	Non-inserted Cations $N_{cat\text{-}lip}$
OMIM-Lact	1.36	0.08
OMIM-Cl	1.27	0.07
OXMIM-Lact	1.40	0.03
OXMIM-Cl	1.33	0.00
TDMIM-Lact	1.36	n/a[b]

[a] Coordination numbers were derived from integration of COM RDFs for pairs of cation ring and lipid phosphates.

[b] All cations were inserted due to special simulation protocol for the TDMIM-Lact system.

Table 4: Number of Water Molecules Coordinated to Cations[a]

IL	Inserted Cations $N_{wat\text{-}cat}$	Non-inserted Cations $N_{wat\text{-}cat}$
OMIM-Lact	6.93	12.42
OMIM-Cl	7.96	12.34
OXMIM-Lact	6.53	11.58
OXMIM-Cl	7.12	11.33
TDMIM-Lact	6.67	n/a[b]

[a] Coordination numbers were derived from integration of COM RDFs for pairs of cation ring and water molecules.

[b] All cations were inserted due to special simulation protocol for the TDMIM-Lact system.

Table 5: Interaction Strengths between Cations and Anions with Individual Coulomb and Lennard-Jones Contributions[a,b]

IL	Ins. cations		Non-ins. cations	
	E_{Coul}	E_{LJ}	E_{Coul}	E_{LJ}
OMIM-Lact	-416_{34}	-0.8_{3}	-448_{28}	-1.06_{8}
OMIM-Cl	-323_{33}	-0.08_{2}	-572_{64}	-0.30_{4}
OXMIM-Lact	-338_{17}	-0.4_{1}	-527_{17}	-1.4_{2}
OXMIM-Cl	-320_{48}	-0.11_{3}	-593_{40}	-0.33_{4}

[a] All values are given in units of kJ mol^{-1}.

[b] Statistical uncertainties of the last digits are given as subscripts.

Table 6: Interaction Strengths between Inserted Cations and Phosphate Groups of Phospholipids with Individual Coulomb and Lennard-Jones Contributions[a,b,c]

IL	E_{Coul}	E_{LJ}	$E_{Coul} + E_{LJ}$
OMIM-Lact	-551_{27}	-41_{1}	-592_{27}
OMIM-Cl	-532_{26}	-37_{2}	-569_{26}
OXMIM-Lact	-573_{23}	-44_{2}	-617_{23}
OXMIM-Cl	-530_{21}	-42_{1}	-571_{21}
TDMIM-Lact	-596_{31}	-43_{1}	-639_{31}

[a] The phospholipid head group was comprised of the lipid phosphate and the attached solvent exposed head group.

[b] All values are given in units of kJ mol^{-1}.

[c] Statistical uncertainties of the last digits are given as subscripts.

Table 7: Surface Area per Molecule, Total Surface Area, Thickness and Roughness of all Simulated Membranes

IL	$A_{mol\text{-}surf}$ [nm^2]	$A_{tot\text{-}surf}$ [nm^2]	d^a [nm]	$r_m{}^b$ [nm]
OMIM-Lact	0.540_2	25.4_1	3.97_4	0.189_4
OMIM-Cl	0.540_1	24.32_6	4.07_7	0.19_2
OXMIM-Lact	0.540_2	24.3_1	4.10_7	0.20_1
OXMIM-Cl	0.560_9	23.9_4	4.1_2	0.19_1
TDMIM-Lact	0.530_2	22.82_7	4.29_4	0.18_1
Pure E. coli	*0.560_8*	*22.4_3*	*4.3_1*	*0.190_8*

[a] Membrane thickness was obtained from difference between average z-coordinate of phosphorus atoms in the two leaflets.

[b] Membrane roughness was determined using eq 4 and subsequent averaging of values for the two leaflets.

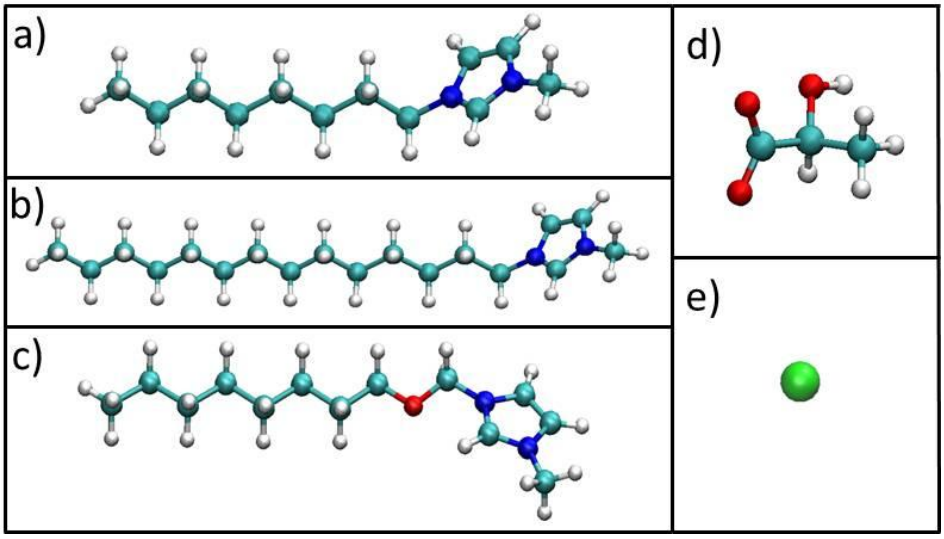

Figure 1: Atomic structures of the ions involved in this study. Cations are shown in structures (a) to (c) while those of anions are shown in (d) and (e). (a) 1-octyl-3-methylimidazolium, (b) 1-tetradecyl-3-methylimidazolium, (c) 1-octyloxymethyl-3-methylimidazolium, (d) l-lactate and (e) chloride. Colour code: hydrogen = white, carbon = turquoise, nitrogen = blue, oxygen = red and chlorine = green.

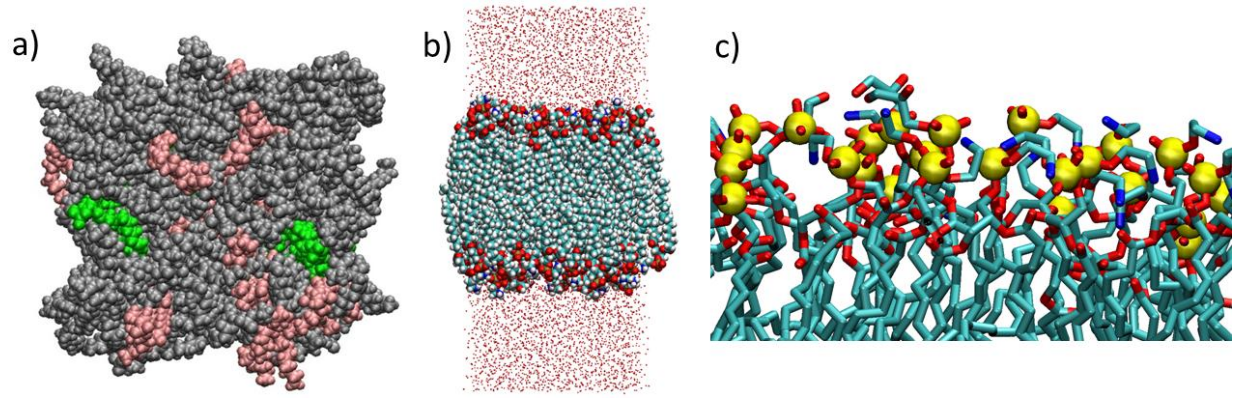

Figure 2: Top (a) and side view (b) of the *E. coli* lipid bilayer model. (c) A magnified side view of a section of the upper layer depicting the positions of phosphorus atoms in the polar region of the bilayer. Color code for (a): POPE = grey, POPG = pink, POPA = green. Color code for (b) and (c): hydrogen = white, carbon = turquoise, nitrogen = blue, oxygen = red and phosphorus = yellow.

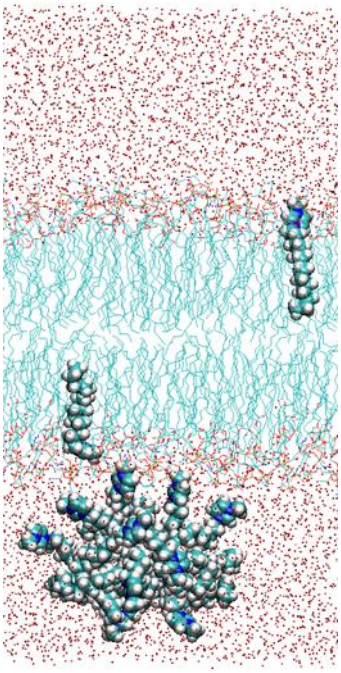

Figure 3: Cation aggregate formation observed in the simulation with TDMIM-Lact. The phospholipid bilayer is shown in the centre with two inserted cations, while the rest of the cations form an aggregate in water as shown in the lower half of the figure.

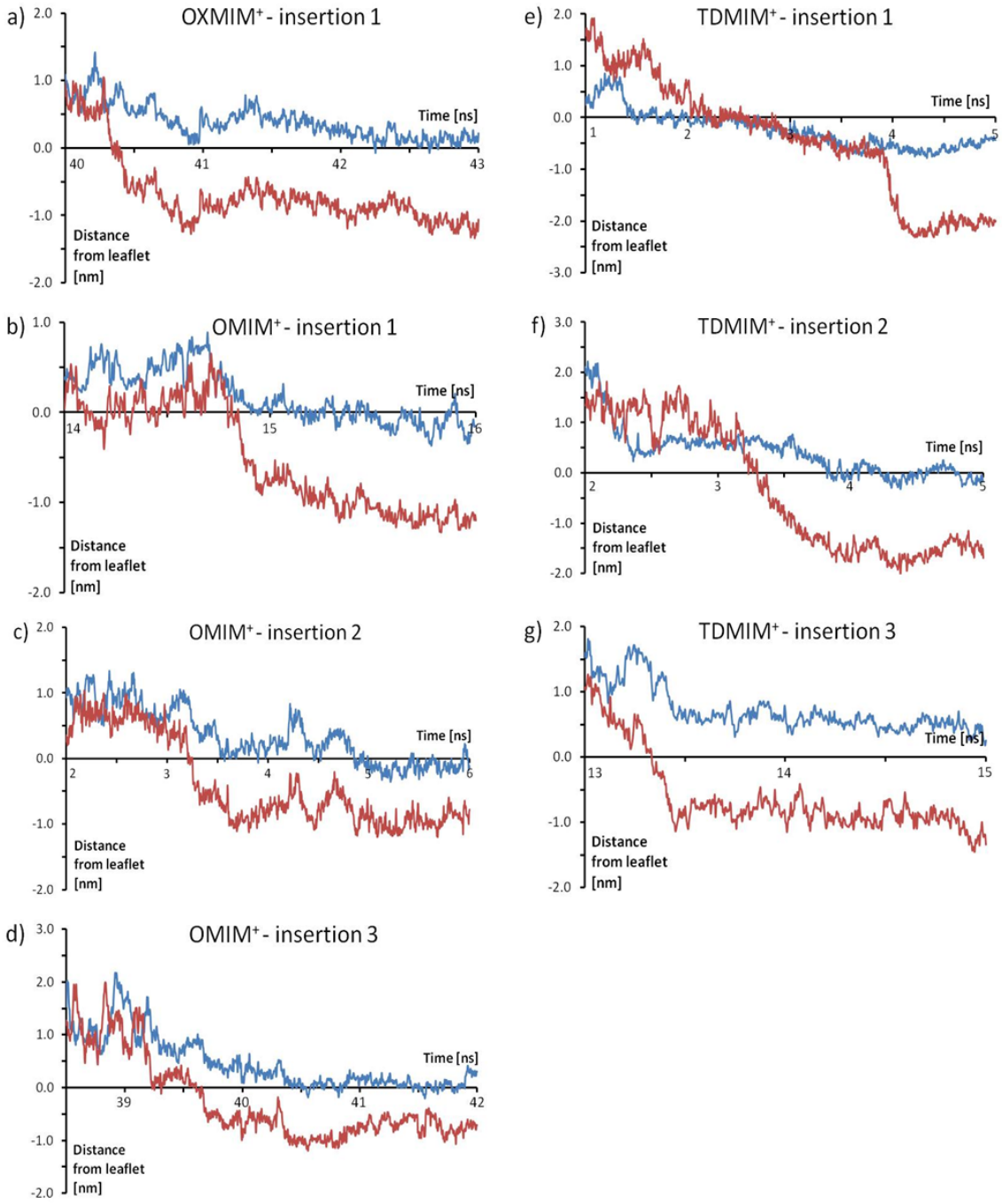

Figure 4: Comparison of the center-of-mass distances of cation head (blue) and tail (red) groups from the membrane layer in z-direction during cation insertion events, respectively. Seven representative instances of cation insertion were selected and are shown in (a) to (g). A tail-first cation insertion mechanism with short cation surface adsorption phases is indicated by these plots.

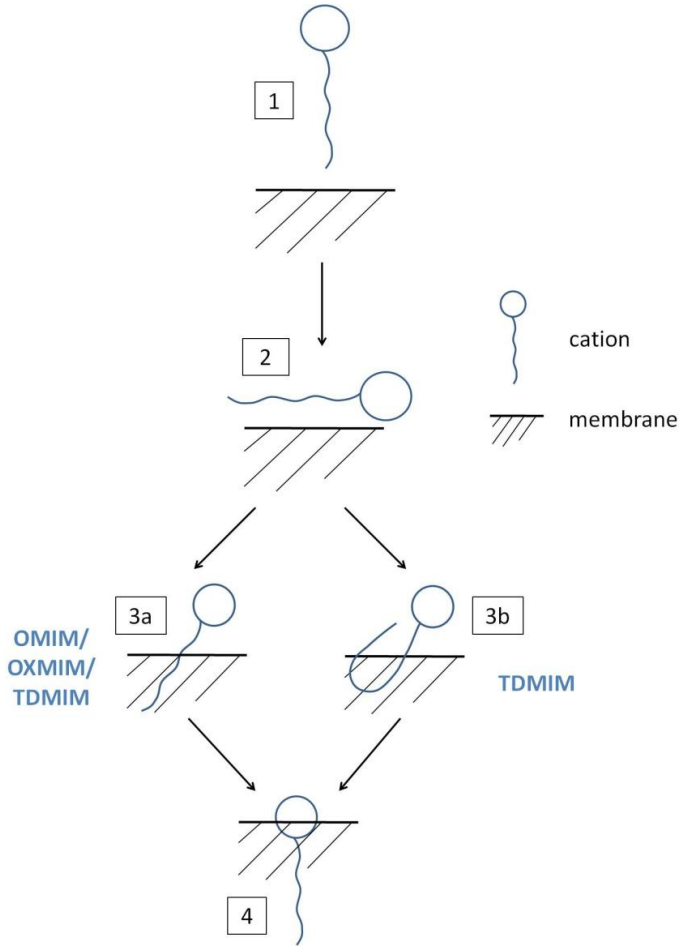

Figure 5: Schematic illustrating the observed cation insertion mechanism. Cations first approach the membrane with their alkyl tail positioned close to the surface, followed by a brief adsorption phase onto the membrane surface for approximately 200 ps, before tilting at an angle to achieve penetration into the membrane. Subsequently, depending on the length of the cation alkyl chain, this chain curls temporarily within the top layer of the membrane, before full extension once the insertion procedure is complete.

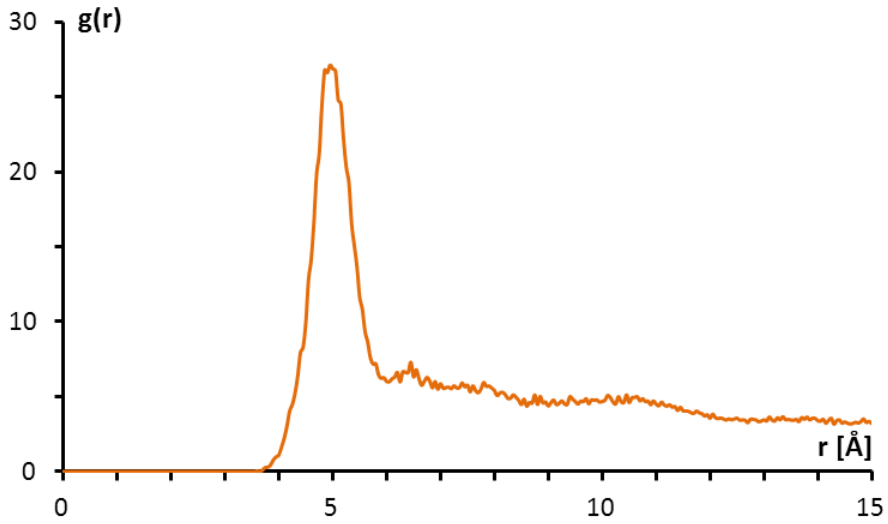

Figure 6: RDF between inserted OMIM cations and phospholipids, with distances measured between the COMs of the imidazolium ring and the lipid phosphate.

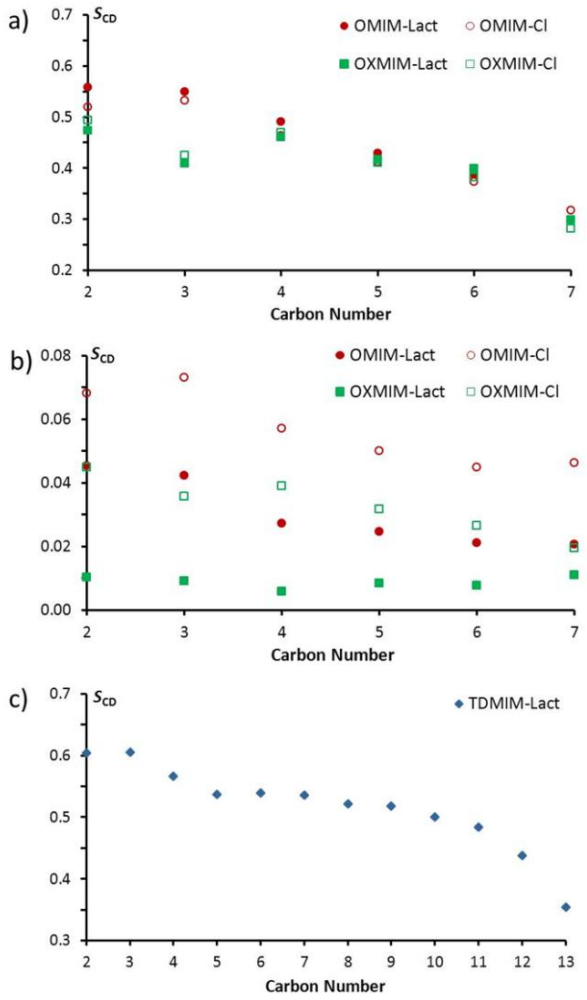

Figure 7: Comparison of deuterium order parameters (S_{CD}) of cation alkyl chain carbons in (a) OMIM and OXMIM inserted into the membrane, (b) OMIM and OXMIM solvated in water, and (c) TDMIM inserted into the membrane. Carbon number 2 refers to the second carbon of the alkyl chain in the case of OMIM and TDMIM, and to the carbon adjacent to the carbon that is directly bonded to the oxygen in the case of OXMIM. The last carbon refers to the carbon adjacent to the terminal methyl group.

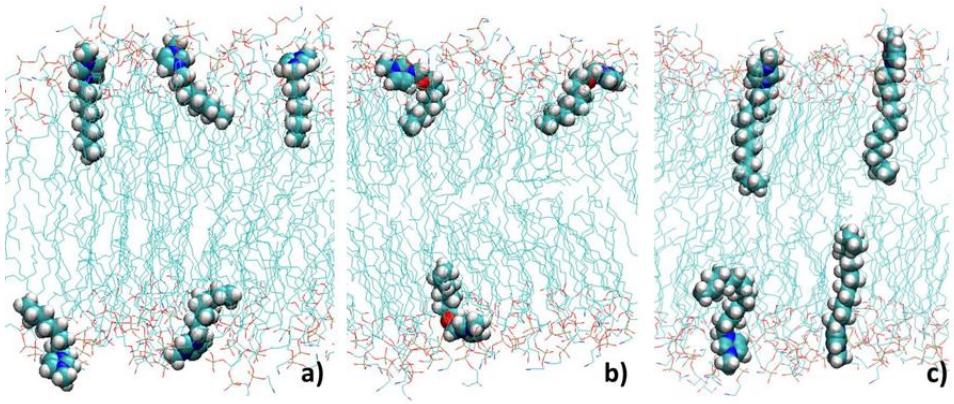

Figure 8: Three representative snapshots of cation insertions for the systems (a) OMIM-Cl, (b) OXMIM-Lact, and (c) TDMIM-Lact. While a flexible alkyl chain can be observed in the case of OMIM and OXMIM, the longer alkyl chain in TDMIM tends to be more straightly aligned on the average.

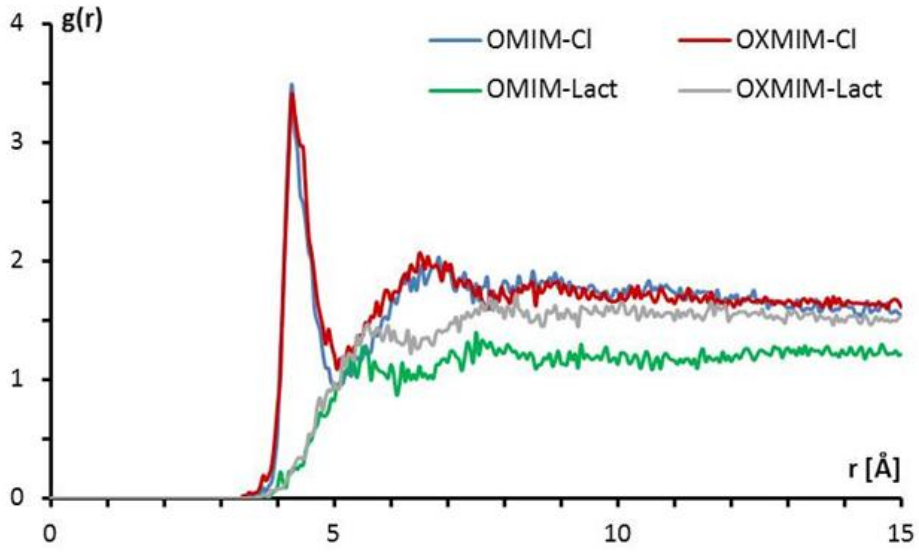

Figure 9: RDFs between non-inserted cations and anions, with distances measured between the COMs of the cation imidazolium ring and the anions.

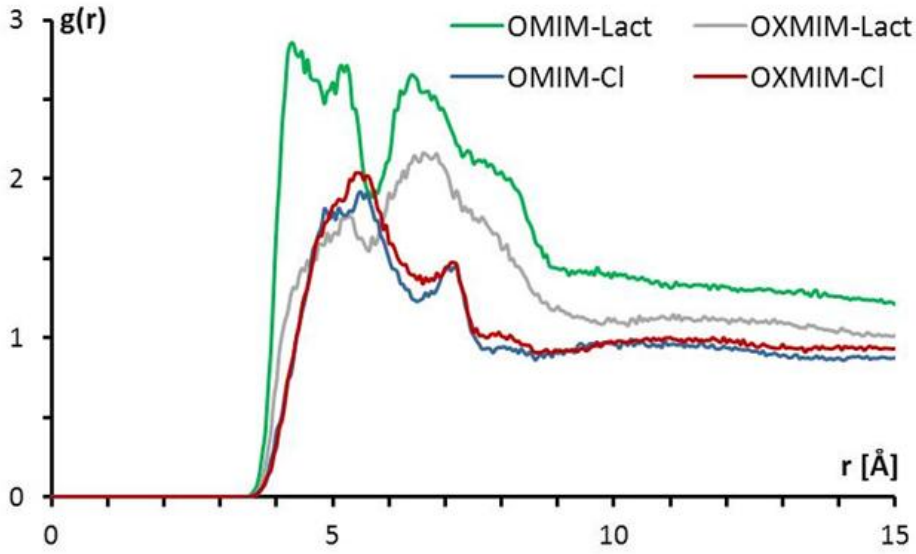

Figure 10: RDF between anions and phospholipids, with distances measured between the COMs of the anions and the lipid phosphate.

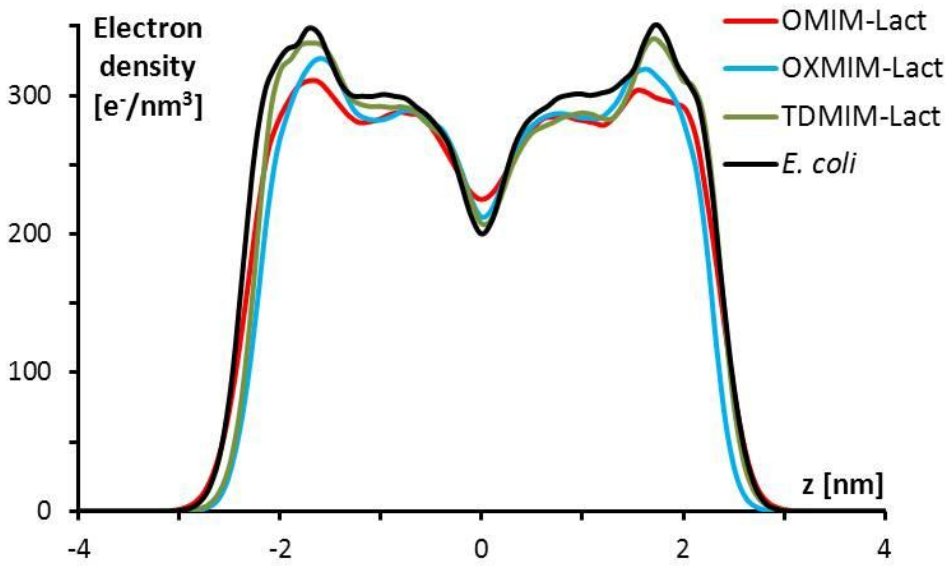

Figure 11: Membrane electron density profiles in the direction perpendicular to the cell membrane, *z*, of various systems superimposed with the unperturbed membrane model of *E. coli*. The centre of the membrane is located at *z* = 0.

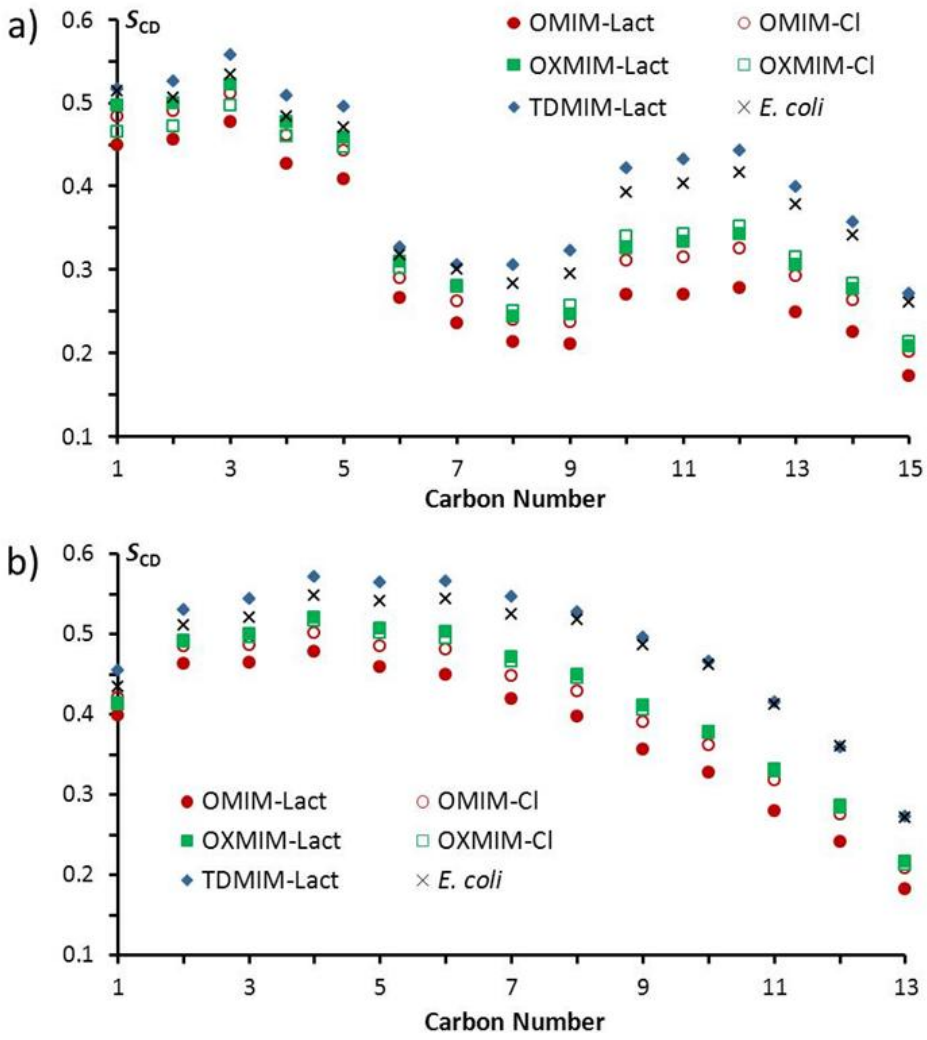

Figure 12: Deuterium order parameters (S_{CD}) of (a) oleoyl and (b) palmitoyl fatty acids in the lipid POPE for the various IL containing systems as well as for the unperturbed *E. coli*. Lipids in the OMIM-Lact, OXMIM-Lact and TDMIM-Lact systems are represented by red filled circles, green filled squares and blue filled diamonds, respectively. Lipids in OMIM-Cl and OXMIM-Cl are labeled with red empty circles and green empty squares, respectively. Lipids in the unperturbed *E. coli* membrane model are represented with a cross. Carbon 1 represents the carbon closest to the polar head group and the last carbon refers to the carbon adjacent to the terminal methyl group.

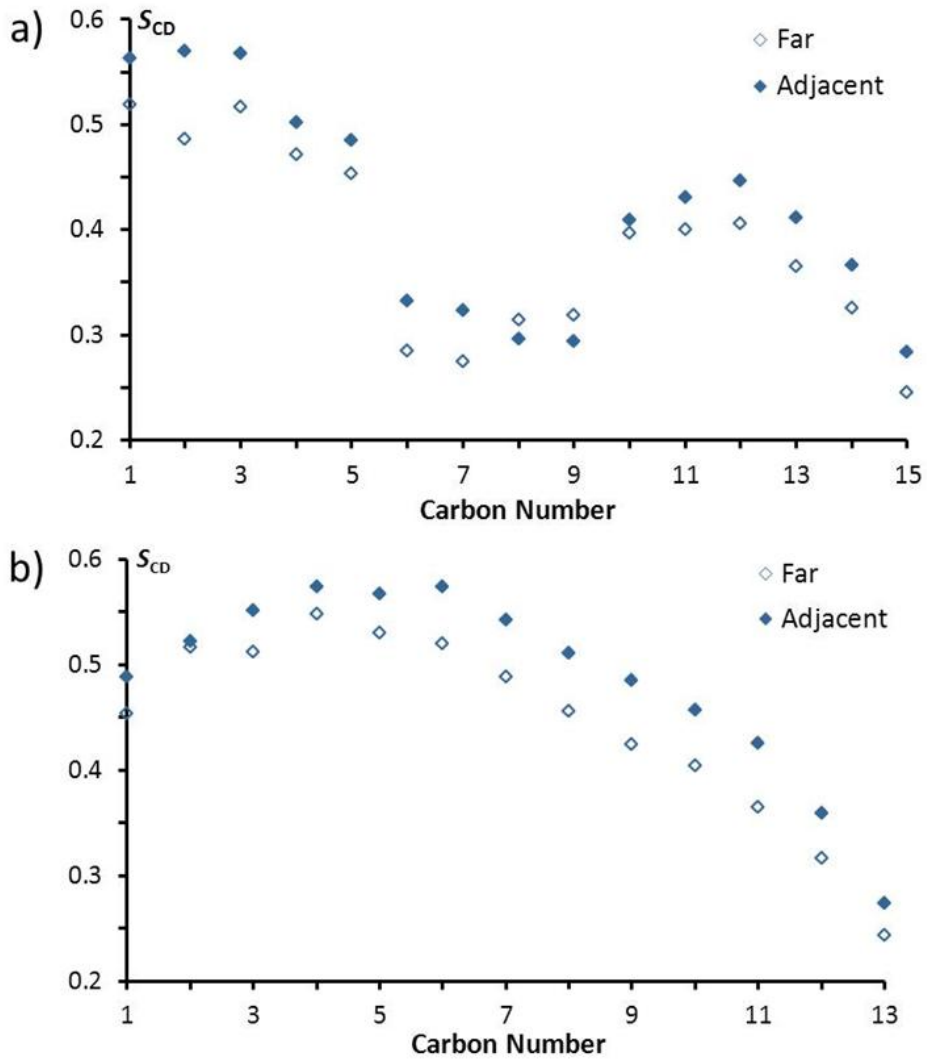

Figure 13: Deuterium order parameters (S_{CD}) of (a) oleoyl and (b) palmitoyl fatty acids in the lipid POPE for the TDMIM-Lact containing system, for lipids within 0.5 nm of inserted TDMIM cations (filled diamonds) and all other lipids (empty diamonds), respectively. Carbon 1 represents the carbon closest to the polar head group and the last carbon refers to the carbon adjacent to the terminal methyl group.